



# Exploration of Quenching Pathways of Multiluminescent Acenes Using the GRRM Method with the SF-TDDFT Method

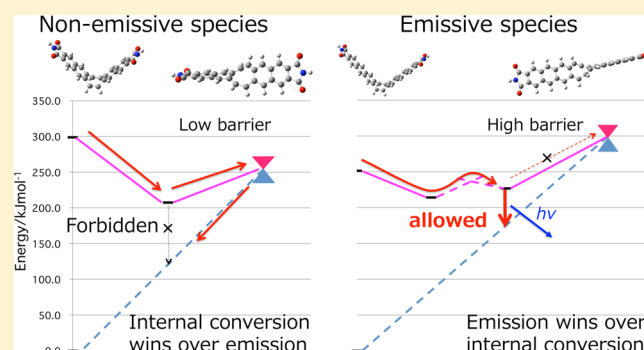
Satoshi Suzuki,<sup>‡</sup> Satoshi Maeda,<sup>§</sup> and Keiji Morokuma<sup>\*,‡</sup>

<sup>‡</sup>Fukui Institute for Fundamental Chemistry, Kyoto University, Kyoto 606-8103, Japan

<sup>§</sup>Department of Chemistry, Faculty of Science, Hokkaido University, Sapporo 060-0810, Japan

**S** Supporting Information

**ABSTRACT:** The quenching pathways were investigated for three types of multiluminescent acene derivatives, which show environment-dependent fluorescence. Spin-flip time dependent density functional theory (SF-TDDFT) combined with the Global Reaction Route mapping (GRRM) strategy is employed to locate minimum-energy conical intersections (MECIs). The energies and geometries of the MECIs relative to the Franck–Condon (FC) state control the difference in fluorescence behavior among the three derivatives. For the molecule with a phenylamide moiety, a MECI with energy lower than the FC state with large geometrical change from V-type to flat structure provides an efficient internal conversion (quenching) pathway in solution. For the same molecule, in a solid, this large geometrical change is inhibited, and the second MECI, with an energy lower than FC but higher than the first MECI requiring only a small geometry change of CH out-of-plane bending, contributes to the quenching. The molecule with the naphthaleneimide moiety has only one low-energy MECI that requires large geometrical change from the V-type to flat structure. Although this MECI provides the quenching pathway in solution, in the solid, this large motion is inhibited, and the molecule will stay in the excited state and emit. The molecule with an anthraceneimide moiety has no conical intersection lower than the FC state, and no quenching pathway is available in solution or solid. In addition, in this molecule, at the local minimum of the excited state, the dipole transition to the ground state is allowed, and this molecule prefers emission rather than internal conversion.



## 1. INTRODUCTION

Owing to their optical and electronic properties,  $\pi$ -conjugated systems have attracted much attention as a functional material. Recently, a series of  $\pi$  systems that consists of a flexible cyclooctatetraene (COT) core and aceneimide wings with different conjugation lengths has been synthesized.<sup>1,2</sup> This system exhibits bent-to-planar conformal change in the excited state. A significant feature of this system is to show environment-dependent fluorescence from a single-component fluorophore. The system gives a blue emission from the V-shaped structure in a polymer matrix or in a frozen solution, a green emission from the planar geometry in solution, and a red emission in the crystalline state.<sup>1,2</sup> The molecule with anthraceneimide wings is emissive both in solution and in the solid state, while the molecule with phenyleneimide has no emission either in solution or in the solid state. For the molecule with a naphthaleneimide moiety, although no fluorescence is observed in the various common organic solvents at room temperature, the compound shows fluorescence in the solid state. The different emission behavior for different acenes has been explained by the difference in the transition dipole moment (TDM). The TDM of phenyleneimide and naphthaleneimide at the  $S_1$  minimum is zero due to symmetry, while that of anthraceneimide at the  $S_1$  minimum

has a finite value. TDM explains why the molecule with an anthraceneimide wing is emissive. However, the difference between phenyleneimide and naphthaleneimide cannot be explained by TDM.

In many photochemical processes such as photochemical reactions and fluorescence quenching, the conical intersections (CIs) play an important role because nonadiabatic transitions from excited states to the ground state take place very efficiently in the vicinity of the CI.<sup>3–8</sup> The CI between two electronic states forms an  $(f - 2)$ -dimensional hypersurface, while individual potential energy surfaces (PESs) form  $f$ -dimensional hypersurfaces, where  $f$  is the internal degree of freedom of a system. Although nonadiabatic transition can take place anywhere near the CI surface, the energy local minimum on the CI hypersurface, the minimum-energy CI (MECI), is a critical point below which CI does not exist and nonadiabatic transition cannot easily take place. In fluorescence, there will be competition between the emission from the local minimum of the excited state controlled by the TDM and quenching through CIs that depends on their geometry, energy, and

**Received:** August 7, 2015

**Revised:** October 28, 2015

**Published:** October 30, 2015

nonadiabatic coupling element. If the path from the Franck–Condon (FC) region to reach a CI is downhill or has a low enough barrier, quenching can compete efficiently with fluorescence.

In order to explain the difference in emission behavior of the present molecules, we explored and located MECIs between  $S_1$  and  $S_0$  for the three aceneimides 1–3 in Figure 1 and

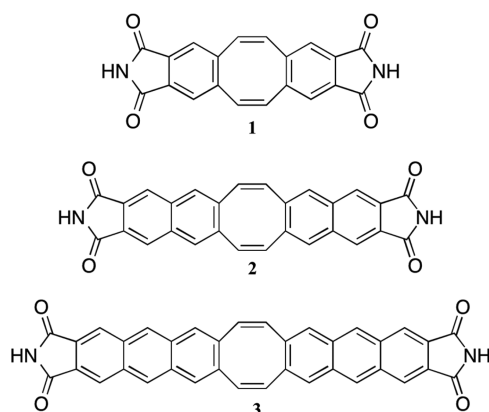


Figure 1. Chemical structure of aceneimide compounds 1–3.

determined possible quenching pathways, starting from the FC region, with the GRRM (Global Reaction Route Mapping) strategy,<sup>9–15</sup> which consists of two independent automatic global search methods, ADDF and AFIR (see ref 12 in detail). The difference in quenching pathway among the three systems would lead to the difference of emission behavior.

Time-dependent density functional theory (TDDFT) is a powerful tool for describing excited states. Among the wave function theories, the multiconfigurational space self-consistent field (MCSCF) method, such as the complete active space self-consistent field (CASSCF), and the multireference perturbation theory, such as the second-order complete active space perturbation theory (CASPT2)<sup>16</sup> and multiconfigurational quasidegenerate perturbation theory (MCQDPT),<sup>17</sup> have been widely used to calculate excited states. CASSCF lacks dynamic correlation and sometimes fails to describe electronic structure properly. The multireference perturbation theory includes dynamic electronic correlation and is usually reliable, but its computational cost is sometimes too large to apply to large molecular systems.

On the other hand, TDDFT is very useful for many cases owing to its “acceptable” accuracy and low computational cost. In the linear response (LR)-TDDFT, excitation energies are determined as poles of the response function. Because the ground state and excited states are treated in a different way, the CI between them cannot be determined in the TDDFT method.

Recently, it has been shown that spin–flip (SF)-TDDFT has a potential ability to obtain the correct CI.<sup>18–21</sup> In SF-TDDFT,  $S_0$  and  $S_1$  states are expressed as excited states from the reference lowest triplet  $T_1$  state that is obtained in the unrestricted Kohn–Sham (UKS) or restricted open-shell Kohn–Sham (ROKS) equation. In the present calculation, ROKS is employed. A significant fault of the SF-TDDFT method is that it often gives spin-contaminated states. To deal with this problem, we checked  $\langle S^2 \rangle$  and the CI coefficients during the optimization. Details are described in a later section.

Section 2 describes the theoretical background and computational methods. In section 3, quenching pathways of each molecule are determined and discussed. The conclusion is given in section 4.

## 2. METHODS AND COMPUTATIONAL DETAILS

In the experiment, *n*-butylimides are used. In the present study, *n*-butyl groups are replaced by hydrogens. Preliminary calculations suggested that the effect of *n*-butyl on the structure and excitation energies is not very significant. For instance, the lowest excitation energy is 2.73 eV with *n*-butyl, while it is 2.72 eV with H. Therefore, this replacement can be justified for qualitative discussion. The equilibrium geometry of each molecule in the  $S_0$  state was optimized at the B3LYP/6-31+G(d) level. Starting from the  $S_0$  equilibrium geometry, the local or global minimum (MIN) for the  $S_1$  state is optimized with TD-B3LYP/6-31+G(d). Throughout the paper, energies and gradients were computed by the GAMESS program.<sup>22</sup>

It turns out that starting the MECI search from the FC geometry by using SF-TDDFT is not necessarily the most efficient as the geometry of MECI is often substantially different from that of the FC geometry and SF-TDDFT states change their nature during optimization. Instead, we used standard restricted and unrestricted DFT methods to calculate  $S_0$  and  $T_1$  states, respectively, and located the approximate minimum-energy point on the seam of crossing (MESX) between  $S_0$  and  $T_1$ . One expects that  $S_0$  and  $T_1$  states have similar shape of potential surfaces if they have the same electron configuration (except for spin). Thus, the  $S_1/S_0$  MECI search from  $S_0/T_1$  MESX is finished with a small number of iterations. This MESX search requires only standard DFT calculations for the lowest singlet and lowest triplet states and avoids SF-TDDFT excited-state calculations. After MESXs were obtained, we searched the  $S_1/S_0$  MECI from each  $S_0/T_1$  MESX.

MESXs are located by adopting the ADDF (anharmonic downward distortion following) search method for the seam model function (SMF) method implemented in the GRRM program.<sup>23</sup> It is worth noting that ADDF search is a method to obtain all possible local minima on a PES. Thus, when we apply the ADDF method to SMF, we can locate many lowest local minima on SMF.

SMF is a function

$$F^{\text{SMF}}(\mathbf{Q}) = \frac{1}{2}[E^{\text{State-1}}(\mathbf{Q}) + E^{\text{State-2}}(\mathbf{Q})] + \frac{[E^{\text{State-1}}(\mathbf{Q}) - E^{\text{State-2}}(\mathbf{Q})]^2}{\alpha} \quad (1)$$

consisting of a mean energy term for the two target PESs,  $E^{\text{State-1}}(\mathbf{Q})$  and  $E^{\text{State-2}}(\mathbf{Q})$ , and a penalty function for their energy difference.  $\mathbf{Q}$  represents the atomic coordinates  $\{Q_i\}$ , and  $\alpha$  is a constant parameter. Minima of SMF correspond to approximate MESX geometries. For each molecule independently, we obtained all important MESXs without guess using a combination of the SMF and ADDF approach. From all of these MESXs (excluding ones with energy higher than  $S_1$  FC), we optimized MECIs. Thus, it is very unlikely that any important MECI is missed. SF-TDB3LYP/3-21G was used for the initial MESXs search, and  $S_1/S_0$  MECIs were reoptimized using the branching plane updating method<sup>11</sup> at the SF-TDB3LYP/6-31+G(d) level, all using the GRRM program.<sup>22</sup> Energies and gradients of the  $S_0$  and  $S_1$  states were calculated

using the SF-TDDFT method with the Tamm–Dancoff approximation implemented in the GAMESS program package. In the SF-TDDFT calculation, the reference triplet state was obtained by the ROKS equation.

One significant fault of SF-TDDFT is that it gives spin-contaminated states. Although expectation values of the total spin-squared operator, namely,  $\langle S^2 \rangle$ , sometimes fluctuate between 0.0 and 2.0, which correspond to pure singlet or triplet states, they often become around 1.0, which indicates strongly mixed states. To determine the nature of SF-TDDFT states, we checked  $\langle S^2 \rangle$  and the CI coefficients during the optimization. With ROKS, there are two open-shell electrons. These two singly occupied orbitals in the reference triplet state should be HOMO and LUMO in the  $S_0$  state. Let us denote the electron configuration using H and L, which correspond to the HOMO and LUMO, and a and b, which mean  $\alpha$  and  $\beta$  spin, respectively. For instance, the reference triplet state becomes HaLa in this notation. The  $S_0$  state should satisfy following two conditions:  $\langle S^2 \rangle \approx 0.0$  and  $C^2(\text{HaHb}) \approx 1.0$ , where  $C$  is a CI coefficient.  $S_1$  consists mainly of the  $(\text{HOMO})^1(\text{LUMO})^1$  configurations. Thus,  $C^2(\text{HaLb}) + C^2(\text{HbLa})$  is usually around 1.0 for this state. We employed the following scheme for the  $S_1/S_0$  MECI search using the SMF ADDF approach:

(1) Starting from ROKS triplet state, obtain the three lowest states by SF-TDDFT. These three states usually are  $S_0$ ,  $S_1$ , and  $T_1$ .

(2) Calculate the following  $T$  index value for each state<sup>13</sup>

$$T = \langle S^2 \rangle + C^2(\text{HaHb}) + C^2(\text{HaLb}) + C^2(\text{HbLa}) + C^2(\text{LaLb}) \quad (2)$$

The  $T$  index should be 3 and 1 for pure  $(\text{HOMO})^1(\text{LUMO})^1$  triplet and singlet states, respectively, and 1 for pure  $(\text{HOMO})^2$  and  $(\text{LUMO})^2$  closed-shell singlet states. This would be 1 for states originating from excitations outside of the  $2 \times 2$  (HOMO) (LUMO) configuration space; such states are mixtures of singlet and triplet states by the nature of the SF-TDDFT method.

(3) Compare three  $T$  values of the lowest three SF-TDDFT states; states with two smaller  $T$  values are judged to correspond to singlet-like states.

(4) Calculate the energy gradients for singlet-like states and generate the next geometry for the  $S_1/S_0$  MECI search.

This state selection scheme based on the  $T$  value does not change the wave function and thus does not avoid spin contamination during geometry optimization. However, near the FC geometry and  $S_1/S_0$  CI, the pure triplet state within the  $2 \times 2$  active space is automatically excluded.

After an  $S_1/S_0$  MECI is obtained, meta-IRC<sup>24</sup> (mass-weighted steepest descent path) calculation on the  $S_0$  state from this MECI was performed to check the direct (without barrier) connectivity of MECI to the  $S_0$  minimum. Geometry optimization on  $S_1$  from the FC geometry as well as that from each MECI was also performed to check whether the FC and the MECI geometries are connected directly (without barrier) to the  $S_1$  minimum. The results will be discussed for each system in the Results and Discussion section.

### 3. RESULTS AND DISCUSSION

#### 3.1. Determination of Critical Points for Molecules 1–

**3. Molecule 1.** Figure 2 shows the structure of important critical points and their energies for molecule 1. Table 1 shows essential geometrical parameters, CC bond distances, and

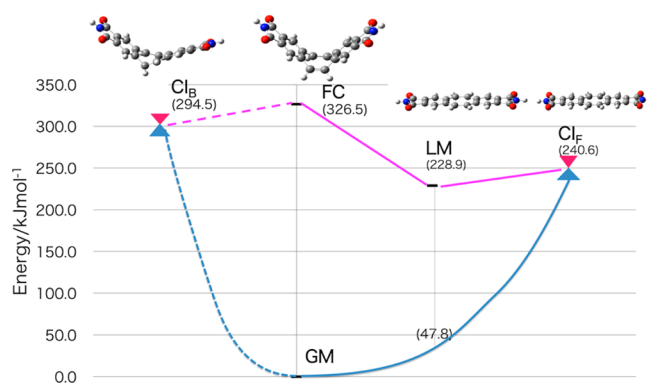


**Figure 2.** Potential energy profile of molecule 1. Solid lines mean that connections between points are confirmed by meta-IRC or geometry optimization. Connections with dotted lines are not confirmed.

CCCX ( $X = \text{C}, \text{H}$ ) dihedral angles of these critical points, and Table 2 gives electronic structure characteristics for these critical points, such as the  $\langle S^2 \rangle$  value, CI coefficients, and  $T$  index.

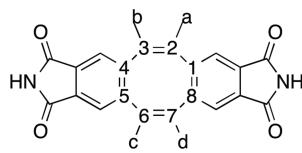
A local minimum LM on the  $S_1$  surface is found near the  $C_{2v}$  FC point (the ground-state minimum GM) with a planar symmetric  $D_{2h}$  structure, in which the  $\text{C2}=\text{C3}$  and weaker  $\text{C4}=\text{C5}$  double bond characters of the  $S_0$  state GM are qualitatively retained, as seen in Table 1. The gradient at FC on  $S_1$  is sloped to the direction of LM, and the meta-IRC from FC confirms that LM is reached without barrier. LM is 97.6  $\text{kJ mol}^{-1}$  lower than FC. The electronic structure characteristics of  $S_1$  at LM in Table 2 indicate that this state is somewhat spin-contaminated, but it can still be assigned to a singlet state. Actually, a triplet  $T_1$  state is relatively close to the  $S_1$  state at this geometry, which causes spin contamination. However, the shape of the  $S_1$  and  $T_1$  PESs would not be much affected by spin mixing.

The optimized MECI  $\text{CI}_F$  also has a planar symmetric  $D_{2h}$  geometry. Comparing with the geometries of GM and LM,  $\text{CI}_F$  shows a profound bond alternation;  $\text{C1}-\text{C2}$  and the other corresponding bonds became short, and  $\text{C2}-\text{C3}$  and  $\text{C4}-\text{C5}$  and the other corresponding bonds became long, totally opposite to the bond character of GM and LM. Thus, one can say that this MECI created is due to the bond alternation of the COT ring. The bond alternation lowers the energy of  $S_1$  and at the same time raises the energy of  $S_0$ , resulting in CIs.  $\text{CI}_F$  is lower in energy than FC by 85.9  $\text{kJ mol}^{-1}$  and is higher than LM only by 11.7  $\text{kJ mol}^{-1}$ . The meta-IRC calculations from FC and  $\text{CI}_F$  on the  $S_1$  surface confirm that both FC and  $\text{CI}_F$  are connected to LM downhill on  $S_1$  without a barrier. The meta-IRC calculation from  $\text{CI}_F$  on the  $S_0$  surface also confirms that  $\text{CI}_F$  is connected to GM downhill on  $S_0$  without a barrier.

We also found a different type of MECI,  $\text{CI}_B$ , which is 32.0  $\text{kJ mol}^{-1}$  lower than FC. We did not explore the lowest-energy path from FC to  $\text{CI}_B$ . However, TDDFT calculations along optimization steps between  $\text{CI}_B$  and GM on the  $S_0$  surface suggest that the barrier between them would not exceed 20.0  $\text{kJ mol}^{-1}$  relative to FC. Therefore,  $\text{CI}_B$  is less favored than  $\text{CI}_F$ , but it is still reachable on the  $S_1$  surface starting from the FC energy and geometry. An optimization from  $\text{CI}_B$  on  $S_0$  suggests that  $\text{CI}_B$  is connected to GM on  $S_0$  without a high barrier.

This  $\text{CI}_B$  with  $C_1$  symmetry shows large out-of-plane bending of two neighboring CH bonds in COT. The dihedral angle  $\text{C5}-\text{C6}-\text{C7}-\text{Hd}$  is  $81.9^\circ$ , with Hd almost perpendicular to the COT  $\text{C5}-\text{C6}-\text{C7}$  plane, and the  $\text{C8}-\text{C7}-\text{C6}-\text{Hc}$  and  $\text{C4}-$

**Table 1.** Important CC Bond Distances and CCCX (X = C, H) Dihedral Angles at the  $S_0$  Global Minimum (FC),  $S_1$  Local Minima (LMs), and  $S_1/S_0$  MECIs (CIs) of Molecules 1–3



molecule				1				2			3			
structure				FC	LM	CI <sub>F</sub>	CI <sub>B</sub>	FC	LM	CI	FC	LM <sub>v</sub>	LM <sub>F</sub>	CI
Dihedral Angle (deg)														
1	2	3	4	0.0	0.0	0.0	−1.0	0.0	0.0	60.6	0.0	0.0	0.0	69.9
2	3	4	5	−58.5	0.0	0.0	−14.1	−57.1	0.0	1.4	−56.4	−38.9	0.0	−0.2
3	4	5	6	0.0	0.0	0.0	−29.7	0.0	0.0	−41.3	0.0	0.0	0.0	−42.1
4	5	6	7	58.5	0.0	0.0	115.1	57.1	0.0	−15.8	56.4	38.9	0.0	−20.7
5	6	7	8	0.0	0.0	0.0	−96.4	0.0	0.0	60.6	0.0	0.0	0.0	70.0
6	7	8	1	−58.5	0.0	0.0	6.1	−57.1	0.0	1.4	−56.4	−38.9	0.0	−0.2
7	8	1	2	0.0	0.0	0.0	18.7	0.0	0.0	−41.3	0.0	0.0	0.0	−42.1
8	1	2	3	58.5	0.0	0.0	6.7	57.1	0.0	−15.8	56.4	38.9	0.0	−20.7
8	1	2	a	−127.6	180.0	180.0	179.5	−129.2	180.0	−177.6	−130.2	−150.5	180.0	178.9
5	4	3	b	127.6	180.0	180.0	174.0	129.2	180.0	−170.5	130.2	150.5	180.0	−172.7
4	5	6	c	−127.6	180.0	180.0	−19.2	−129.2	180.0	−177.5	−130.2	−150.5	180.0	−178.9
1	8	7	d	127.6	180.0	180.0	−172.3	129.2	180.0	−170.6	130.2	150.5	180.0	−172.7
4	3	2	a	−173.7	180.0	180.0	−173.8	−173.6	180.0	−137.3	−173.3	−170.6	180.0	−129.2
1	2	3	b	173.7	180.0	180.0	171.0	173.6	180.0	−127.3	173.3	170.6	180.0	−117.5
8	7	6	c	−173.7	180.0	180.0	37.9	−173.6	180.0	−137.3	−173.3	−170.6	180.0	−129.2
5	6	7	d	173.7	180.0	180.0	81.9	173.6	180.0	−127.3	173.3	170.6	180.0	−117.4
Bond Distance (Å)														
	1	2		1.422	1.473	1.359	1.422	1.481	1.415	1.374	1.480	1.455	1.424	1.366
	2	3		1.428	1.353	1.468	1.428	1.344	1.403	1.452	1.344	1.364	1.400	1.465
	3	4		1.410	1.473	1.362	1.410	1.481	1.415	1.372	1.480	1.455	1.424	1.369
	4	5		1.462	1.430	1.521	1.462	1.432	1.478	1.488	1.444	1.437	1.474	1.489
	5	6		1.406	1.472	1.359	1.406	1.481	1.415	1.374	1.480	1.455	1.419	1.366
	6	7		1.437	1.353	1.468	1.437	1.344	1.403	1.452	1.344	1.364	1.397	1.465
	7	8		1.389	1.472	1.362	1.389	1.481	1.415	1.372	1.480	1.455	1.419	1.369
	8	1		1.497	1.430	1.521	1.497	1.432	1.478	1.488	1.444	1.437	1.474	1.489
symmetry				$C_{2v}$	$D_{2h}$	$D_{2h}$	$C_1$	$C_{2v}$	$D_{2h}$	$C_2$	$C_{2v}$	$C_{2v}$	$C_{2v}$	$C_2$

**Table 2.**  $\langle S^2 \rangle$  Value, CI Coefficients, and  $T$  Index Values for  $S_0$  and  $S_1$  States at the  $S_0$  Global Minimum (FC),  $S_1$  Local Minima (LMs), and  $S_1/S_0$  MECIs (CIs) of Molecules 1–3

molecule		1				2			3			
structure		FC	LM	CI <sub>F</sub>	CI <sub>B</sub>	FC	LM	CI	FC	LM <sub>v</sub>	LM <sub>F</sub>	CI
$S_0$	$\langle S^2 \rangle$	0.003	0.005	0.410	0.148	0.013	0.009	0.030	0.015	0.005	0.013	0.015
	CI(HaHb)	0.999	−0.998	−0.821	−0.938	−0.994	0.997	−0.459	−0.992	0.998	−0.993	0.836
	CI(HaLb)	0.000	0.000	0.556	−0.137	0.000	0.000	−0.671	0.000	0.000	0.000	0.382
	CI(HbLa)	0.000	0.000	0.079	−0.094	0.000	0.000	0.571	0.000	0.000	0.000	−0.379
	CI(LaLb)	0.000	0.000	−0.080	0.000	0.000	0.000	0.000	0.000	0.000	0.000	0.000
	$T$ index	1.001	1.001	1.405	1.056	1.000	1.001	1.001	1.001	1.001	1.001	1.001
$S_1$	$\langle S^2 \rangle$	0.062	0.088	0.253	0.930	1.013	0.079	0.015	0.308	1.002	1.061	0.067
	CI(HaHb)	0.000	0.000	−0.188	−0.104	0.000	0.000	0.882	0.000	0.000	0.000	−0.537
	CI(HaLb)	0.578	0.549	0.000	0.980	0.000	0.562	−0.312	−0.597	0.000	−0.189	0.000
	CI(HbLa)	−0.813	−0.833	0.891	0.000	0.000	−0.823	0.338	0.584	0.000	−0.130	−0.498
	CI(LaLb)	0.000	0.000	−0.403	0.065	0.000	0.000	0.000	0.000	0.000	0.000	0.665
	$T$ index	1.057	1.083	1.244	1.906	1.013	1.071	1.005	1.006	1.002	1.114	1.046

C5–C6–Hc are 37.9 and  $-19.2^\circ$ , respectively, with the Hc very much twist-bent from the COT C5–C6–C7 plane (Table 1). A CI similar to this has been found for COT<sup>25</sup> and is also similar to the twisted CI of stilbene.<sup>20,26</sup> As seen in Table 2, at this CI,  $S_1$  and  $T_1$  are strongly spin-contaminated;  $\langle S^2 \rangle$  for the  $S_1$  and  $T_1$  states is 0.93 and 1.05, respectively (Table 2). The  $T$  index for the SF-TDDFT state 2 is smaller than that of state 3,

and hence, state 2 is assigned to  $S_1$  and state 3 to  $T_1$ . Because the energy difference between states 2 and 3 is only 28 kJ mol<sup>−1</sup>, the crossing between  $S_0$  and the spin-pure  $S_1$  state should have a similar geometry to the crossing structure obtained for the heavily spin-mixed state. To examine these states, single-point (4,4) CASSCF calculation is also performed. HOMO−1, HOMO, LUMO, and LUMO+1 are taken into

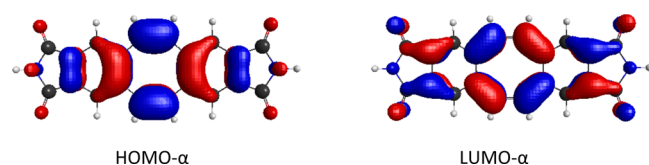


**Table 3.** Energy,  $\langle S^2 \rangle$  Value, CI Coefficients, and  $T$  Index Values for  $T_1$ ,  $S_0$ ,  $S_1$ , and  $T_2$  States of SF-TDDFT at the  $S_1/S_0$  MECI ( $CI_B$ ) of Molecule 1 along with (4,4)-CASSCF Energy and CI Coefficients for  $S_0$ ,  $T_1$ , and  $S_1$  States at the Same Geometry

	SF-TDDFT				2SA-(4,4)CASSCF		
	$T_1$ (ROKS state)	$S_0$	$S_1$	$T_1$	$S_0$	$T_1$	$S_1$
$\Delta E$ (kJ/mol)	0.0	30.5	30.5	58.4	0.0	26.0	60.1
$\langle S^2 \rangle$	2	0.1482	0.9301	1.0531	0	2	0
CI(HaHb)	0.0000	−0.9380	−0.1043	0.1132	−0.0769	0.0000	0.9046
CI(HaLb)	0.0000	−0.1368	0.9801	0.0000	0.6238	−0.6068	0.0000
CI(HbLa)	0.0000	−0.0944	0.0000	−0.9626	0.6238	0.6068	0.0000
CI(LaLb)	0.0000	0.0000	0.0653	0.0581	0.0000	0.0000	0.1349
$T$ index		1.056	1.906	1.996			

active orbitals, and  $S_0$  and  $S_1$  states are averaged. As shown in Table 3, the  $S_0$  state in SF-TDDFT corresponds to the  $S_1$  state in CASSCF. On the other hand,  $S_1$  and  $T_1$  states in SF-TDDFT correspond to linear combinations of  $S_0$  and  $T_1$  states in CASSCF. This reflects the fault of the SF-TDDFT method; for more quantitative description of these states, a more accurate and contamination-free method such as CASPT2 is needed.

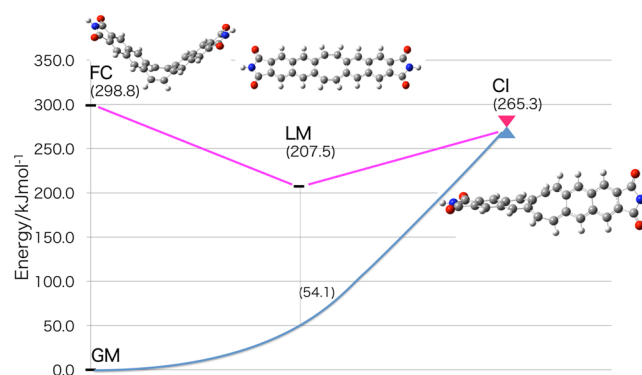
Interestingly, at both  $CI_F$  and  $CI_B$ , deformation mainly takes place on the COT ring. In a preliminary calculation with a small basis set, we also found other CIs with out-of-plane CH bending of benzene ring hydrogens. However, these types of CIs have much higher energy and will not contribute to the quenching of luminescence, and therefore, such CIs will not be discussed in the present paper. The reason why the deformation takes place on the COT ring comes from the nature of the excited state. Figure 3 shows two singly occupied

**Figure 3.** Two singly occupied orbitals (called HOMO- $\alpha$  and LUMO- $\alpha$ ) from the ROKS triplet reference calculation at the  $S_1$  LM geometry of molecule 1.

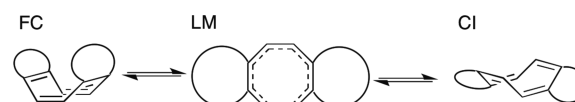
orbitals (called HOMO- $\alpha$  and LUMO- $\alpha$ ) from the ROKS triplet reference calculation at the  $S_1$  LM geometry of molecule 1. These MOs are mainly localized in the COT ring and clearly represent bond alternation within the COT ring upon excitation from the HOMO to LUMO in  $S_1$ . A small density on the phenyl carbon next to the COT ring suggests that bending of this CH bond may result in a high-energy CI.

**Molecule 2.** Figure 4 and Table 1 show the structure of important critical points and their energies for molecule 2. For molecule 2, a local minimum LM with  $D_{2h}$  symmetry is found on  $S_1$ , which is similar to the  $S_1$  local minimum LM of 1. Comparing these two molecules, we can see some differences in bond distances. In molecule 1, bond distances of 1–2, 2–3, and 4–5 are 1.473, 1.353, and 1.430 Å, respectively. In molecule 2, they are 1.415, 1.403, and 1.478 Å, respectively; the bond distance alternation is very much reduced.

On the other hand, the structure of MECI CI is quite different from either of the two MECIs,  $CI_F$  and  $CI_B$ , of molecule 1. At this CI, the COT has made a major structural change from the  $S_0$  GM. The larger V-shaped bend of the COT ring in the  $S_0$  GM has disappeared completely and been replaced by a  $C_2$  pseudo-tub-shaped conformation of COT with aryl groups attached on the side of the tub (Figure 5). This

**Figure 4.** Potential energy profile of molecule 2. Solid lines mean that connections between points are confirmed by meta-IRC or geometry optimization. Connections with dotted lines are not confirmed.

distortion is quite different from those of 1,  $CI_F$  promoted by bond alternation, and  $CI_B$  associated with the C–H out-of-plane bending.

**Figure 5.** Schematic representation of critical points of molecule 2.

Another flat CI, similar to  $CI_F$  of 1, may also exist. We also tried to find such a CI from LM, but finally we obtained only this pseudo-tub CI. We conclude that such a flat CI in molecule 2 does not exist or is substantially higher in energy. This CI for molecule 2 is lower than the  $S_1$  FC by 33.5 kJ mol<sup>−1</sup> but 57.8 kJ mol<sup>−1</sup> higher than  $S_1$  LM. Although the required energy is not so small, this CI is still accessible from FC. The meta-IRC calculations from FC and CI on the  $S_1$  surface confirm that both FC and CI are connected to LM downhill on  $S_1$  without a barrier. The meta-IRC calculation from CI on the  $S_0$  surface also confirms that CI is connected to GM downhill on  $S_0$  without a barrier.

Different from 1, the pseudo-tub-shaped CI is the only MECI lower than FC. In preliminary calculation with a small basis set, we also found other CIs that have strong CH out-of-plane bending as in  $CI_B$  of 1. However, this CI is much higher in energy than FC. Thus, we will not consider these high-energy CIs in the later discussion.

Table 2 indicates that both LM and CI are nearly pure singlet states with small  $\langle S^2 \rangle$  values and the  $T$  indices of nearly 1. At LM,  $S_0$  is a closed shell, and  $S_1$  is an open-shell singlet, and at CI, the two singlets are fully mixed.

**Molecule 3.** There is a noticeable difference between molecule 3 and molecules 1 and 2. For molecule 3, two  $C_{2v}$  local minima for  $S_1$  state were found (Figure 6 and Table 2). As

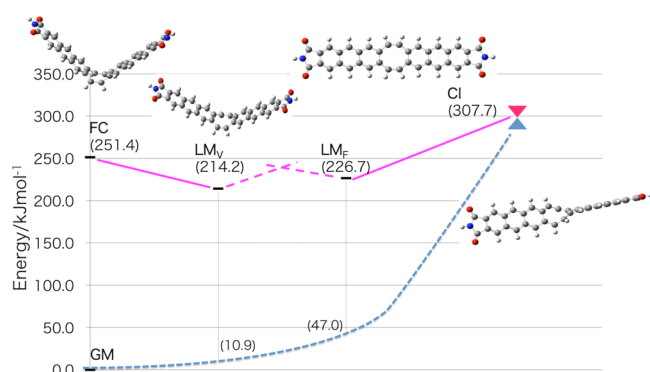


**Figure 6.** Potential energy profile of molecule 3. Solid lines mean that connections between points are confirmed by meta-IRC or geometry optimization. Connections with dotted lines are not confirmed.

found previously,<sup>2</sup> there is one local minimum  $LM_V$  that has a shallow V shape and another local minimum  $LM_F$  with flat  $C_{2v}$  geometry.  $LM_V$  is lower in energy by 12.5 kJ mol<sup>-1</sup> than  $LM_F$ . This is different from a previous study, in which relaxed scan found  $LM_F$  slightly lower than  $LM_V$ .<sup>2</sup> Because the differences between two geometries are as small as the typical error of TDDFT (around 0.1 eV, namely, 10 kJ mol<sup>-1</sup>),<sup>27</sup> we will not discuss this difference further.

At the FC  $C_{2v}$  V-shaped structure, the lowest singlet excited state  $S_1$  is  $^1A_2$ . Following the meta-IRC from FC,  $LM_V$ , still with a V-shaped structure with a smaller bending angle, is reached with  $^1A_2$  as  $S_1$ . As the molecule become even more planar,  $^1B_2$  becomes lower than  $^1A_2$ . At the second  $S_1$  minimum  $LM_F$ , the molecule is coplanar, and the first excited state is  $^1B_2$ . The electronic transition (emission) from  $^1B_2$  to  $S_0$  ( $^1A_1$ ) is allowed, while that from  $^1A_2$  to  $S_0$  is forbidden. Thus, molecule 3 can give emission from the second  $S_1$  minimum  $LM_F$  but not from the first minimum  $LM_V$ . The calculated vertical emission energy (without zero-point energy correction) from  $LM_F$  is 179 kJ mol<sup>-1</sup>, while that of experiment in solution is 230 kJ mol<sup>-1</sup> (520 nm).

Between the two minima  $LM_V$  and  $LM_F$ , there should be a transition state due to avoided crossing of the two electronic states. It is not easy to describe this avoided crossing with the SF-TDDFT method, and a search based on SF-TDDFT did not give a reliable TS structure. However, from an approximate scan of the two states, one can say that the barrier between  $LM_V$  and  $LM_F$  would be less than 20 kJ mol<sup>-1</sup>. The process going from FC through  $LM_V$  to  $LM_F$  would be a viable step.

In molecule 3, the COT moiety is antiaromatic in the ground state. Thus, conjugation is divided into two parts. On the other hand, at the  $LM_F$ , the COT moiety becomes planar, and conjugation becomes enlarged to the whole system. This delocalization stabilizes the  $^1B_2$  state, and the order of excited states is switched.

One MECI, labeled CI, has been found for molecule 3. CI is higher in energy than the FC structure FC by 56.3 kJ mol<sup>-1</sup>. This structure CI consists of two nearly planar acene structures that are connected by a nearly perpendicularly twisted COT structure, similar to the CI structure of 2. A flat CI like 1 could not be found, which is the same result as 2. It is interesting to follow the structure change of molecule 3 on  $S_1$ : deeply V-

shaped FC, followed by shallowly V-shaped  $LM_V$ , coplanar  $LM_F$ , and twisted CI.

One notices that CI of molecule 2 is lower than FC by 33.5 kJ mol<sup>-1</sup>, while CI of molecule 3 is higher than FC by 56.3 kJ mol<sup>-1</sup>. As shown in Table 1, structures of CI for 2 and 3 are similar. Thus, it is difficult to explain this energy difference from a structural point of view. To verify electronic structure at CIs, we performed  $S_0/S_1$  state-average (4,4) CASSCF/6-31+(d) single-point calculation at the MECI CI for both molecule 2 and 3. In Figure 7, four natural orbitals (NOs) of 2 and 3 are

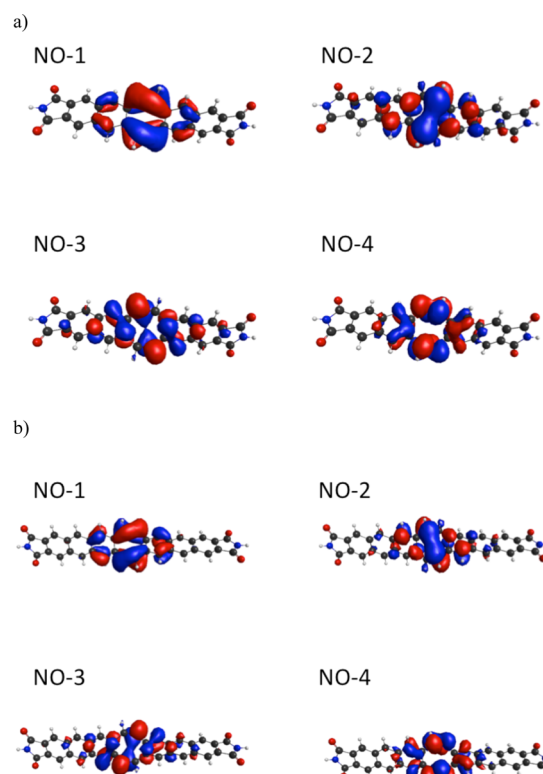


**Figure 7.** (a) Two-state SA (4,4) CASSCF NOs at CI for molecule 2. The occupation number for each NO for state 1 is 1.882, 1.405, 0.612, and 0.100, respectively. (b) Two-state SA (4,4) CASSCF NOs at CI for molecule 3. The occupation number for each NO is 1.799, 1.329, 0.705, and 0.167, respectively.

shown (isovalues = 0.025). Apparently, their orbitals are very similar, and the natural orbital occupation numbers (NOONs) are also similar. For molecule 2, the NOON for each NO is 1.882, 1.405, 0.612, and 0.100, respectively; for molecule 3, the NOON for each NO is 1.799, 1.329, 0.705, and 0.167, respectively. We can conclude that the difference between electronic structures on CI for 2 and 3 is not large enough to explain energetics on CI.

One significant difference, as shown in Figure 8, between 2 and 3 is the symmetry of LMs. As shown in Table 1, LM for 2 is a rectangle belonging to  $D_{2h}$ , while  $LM_F$  for 3 loses  $C_2$  symmetry around the  $z$ -axis and is a trapezoid belonging to  $C_{2v}$ . On the other hand, the CIs for both 2 and 3 are a twisted rectangle, possessing  $C_2$  rotational symmetry around the  $z$ -axis. Now, we introduce for 3 a hypothetical  $D_{2h}$  structure  $H_{D2h}$  by symmetrizing the  $LM_F$   $C_{2v}$  structure. The energy difference between CI and  $LM_F$  can now be rewritten as

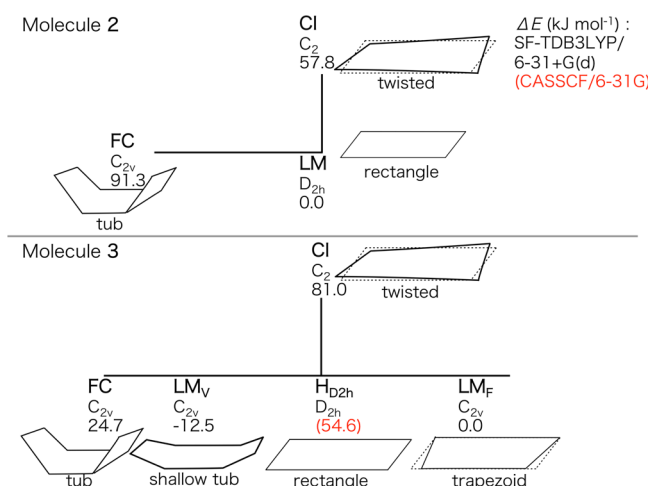


**Figure 8.** Schematic illustration of geometries (symmetries) and energies of critical points of molecules 2 and 3, at the SF-TDB3LYP/6-31+G(d) level, except for the red number in CASSCF/6-31G. See the text for details.

$$E(\text{CI}) - E(\text{LM}_F) = [E(\text{CI}) - E(\text{H}_{D_{2h}})] + [E(\text{H}_{D_{2h}}) - E(\text{LM}_F)] \quad (3)$$

This divides the LM<sub>F</sub> to CI geometry change into the trapezoid-to-rectangle deformation (LM<sub>F</sub> to H<sub>D<sub>2h</sub></sub>) and the twisting of the rectangle (H<sub>D<sub>2h</sub></sub> to CI). Unfortunately, the SF-TDDFT calculation at H<sub>D<sub>2h</sub></sub> did not converge. Therefore, instead, we estimated the energy of the hypothetical D<sub>2h</sub> structure H<sub>D<sub>2h</sub></sub> as follows. LM<sub>F</sub> was optimized with state-specific (4,4)-CASSCF/6-31G for the S<sub>1</sub> state (<sup>1</sup>B<sub>2</sub> in C<sub>2v</sub> symmetry), and then the D<sub>2h</sub> structure H<sub>D<sub>2h</sub></sub> was obtained by symmetry-constrained optimization with the same method as that for the S<sub>1</sub> state (<sup>1</sup>Ag). The energy difference between H<sub>D<sub>2h</sub></sub> and LM<sub>F</sub>, the stabilization energy due to rectangle-to-trapezoid distortion, is calculated to be 54.6 kJ mol<sup>-1</sup> at this level. Therefore, one can conclude that the CI–LM energy difference in molecule 3 is much larger than that in molecule 2 because LM<sub>F</sub> of 3 is stabilized by 54.6 kJ mol<sup>-1</sup> from the hypothetical rectangular structure and corresponding electronic structure, while LM of 2 already has a rectangular structure. Molecule 2 in the LM structure in the S<sub>1</sub> excited state prefers to keep each of the smaller naphthalene groups symmetric around the COT core, while molecule 3 in the LM<sub>F</sub> structure in the S<sub>1</sub> excited state prefers to distort each of the larger anthracene groups into a trapezoid.

### 3.2. Quenching Pathway for Three Types of Molecule.

In molecule 1, as seen in Figure 2, after vertical excitation, the minim-energy path takes the system preferentially to the S<sub>1</sub> LM. The electronic transition (emission) from S<sub>1</sub> to S<sub>0</sub> is forbidden by symmetry, and the molecule cannot emit from S<sub>1</sub> LM. From LM, the molecule moves easily to the MECI CI<sub>F</sub>, through which it moves on to the S<sub>0</sub> ground state to reach the S<sub>0</sub> global minimum. This quenching pathway is driven by the large geometry from the V shape in FC to the coplanar shape in LM and CI<sub>F</sub>. This geometry change is accompanied by the COT bond alternation caused by electronic excitation. This quenching pathway should be the most preferable in solution and is likely to occur in high probability as the meta-IRC on S<sub>1</sub> from FC leads to LM and to CI<sub>F</sub> without any barrier. In addition, there is another MECI CI<sub>B</sub> in the different direction of geometry distortion. Although CI<sub>B</sub> is also lower in energy

than FC, the pathway toward CI<sub>B</sub> from FC is not on the steepest decent path and should be accessible from FC with some activation energy. This path not on the minimum-energy pathway may contribute but is not likely to compete against the steepest descent quenching path via MECI CI<sub>F</sub> in the gas phase or in solution.

In solid, however, large structural changes should be inhibited by the surroundings. Thus, CI<sub>F</sub> that requires a large geometry change from the FC V structure to a planar structure may not be reachable. However, CI<sub>B</sub> is lower in energy than FC and requires relatively small structural change (a CH out-of-plane bending retaining the V-shape structure). Thus, CI<sub>B</sub> is expected to be reachable even in the solid state. Therefore, we propose that the quenching of molecule 1 via CI<sub>B</sub> is still possible in solid, explaining qualitatively the experimental finding of no emission either in solution or in solid for molecule 1.

On the other hand, in molecule 2, there is only one type of MECI, CI, with lower energy in the vicinity of FC. No CI for 2, similar to CI<sub>B</sub> in molecule 1, could not be located in the GRRM SMF search, suggesting that this, if it exists, is substantially higher in energy than FC. The electronic transition (emission) from S<sub>1</sub> to S<sub>0</sub> is forbidden by symmetry and should be weak. The molecule 2 moves easily to the MECI CI, through which the molecule moves on to the S<sub>0</sub> ground state to reach the S<sub>0</sub> ground minimum, as in molecule 1. This should be the favorable quenching pathway in the gas phase and in solution. As discussed for molecule 1, this pathway of quenching would be prohibitive in solid also for molecule 2. This pathway from the V-shape FC through coplanar LM to twisted CI requires a large geometrical change and will be inhibited by surroundings. The above argument qualitatively explains why molecule 2 is nonemissive in solution and is only weakly emissive in solid.

In molecule 3, the situation is totally different from 1 and 2. At LM<sub>F</sub>, the transition between S<sub>1</sub> and S<sub>0</sub> is allowed by symmetry. In addition, the barrier toward CI is high enough. Thus, in this molecule, fluorescence is more likely to take place than internal conversion in either the solution or solid, consistent with experimental observations.

## 4. CONCLUSION

We have explored quenching pathways of three multi-luminescent molecules using SF-TDDFT in conjunction with the GRRM ADDF automatic search method for MECI and proposed different quenching mechanisms for three different molecules 1, 2, and 3. As a referee suggested, it may be hard to believe that the photochemistry of these structurally similar molecules is qualitatively as different as reported. A standard search from a guess would have missed this difference. The unbiased and global search of MECIs by the GRRM ADDF method demonstrated that dramatic change in MECI characteristics and emission behavior is exactly what is taking place going from molecule 1 to 2 to 3.

Molecule 1 with phenyleneimide has two low-energy MECIs, CI<sub>F</sub> and CI<sub>B</sub>. In contrast to the strongly V-shaped FC structure FC, CI<sub>F</sub> has a flat structure and is lower than FC by 86 kJ mol<sup>-1</sup> and is connected via the local minimum LM (12 kJ mol<sup>-1</sup> lower than CI<sub>F</sub>) to FC directly without barrier. Thus, the excited molecule should be quenched very easily in the gas phase and in solution in which a large geometrical distortion from FC to CI<sub>F</sub> can be accomplished. The other CI CI<sub>B</sub> is energetically less favorable than CI<sub>F</sub> and is not likely to compete against the quenching from CI<sub>F</sub>. However, this CI involves only CH out-



of-plane motion that requires smaller geometry changes than the flat  $\text{CI}_F$ . Thus,  $\text{CI}_B$  can be reached even in solid and provides the quenching pathway in solid.

Molecule **2** with naphthaleneimide has only one conical intersection  $\text{CI}$  in the region that is lower in energy than the  $\text{FC}$  state. This  $\text{CI}$  shows a twisted structure with acene wings on the side of the tub-shaped cyclo-octatetraene ring and requires a large molecular motion. Thus, this  $\text{CI}$  is the quenching pathway in the gas phase and solution. However, in solid, this  $\text{CI}$  cannot be reached, and molecule **2** should be able to stay in the excited state and emit.

Different from the two molecules above, molecule **3** with anthraceneimide has no  $\text{CI}$  that is lower in energy than the  $\text{FC}$  state. Therefore, the quenching is not available in solution as well as in solid. Moreover, at the equilibrium structure in the  $S_1$  state, transition from  $S_1$  to  $S_0$  is allowed by symmetry. Thus, this molecule is emissive even in solution.

We can conclude that the difference of emission behavior is determined by the difference of structures and energies of  $\text{CIs}$ . We succeeded in qualitatively explaining different emission behavior of three multiluminescent molecules. The present method of determining the structures and energies of low-energy  $\text{CI}$  using the GRRM strategy should be applicable to other photofunctional molecules, and such studies are in progress. Nonadiabatic molecular dynamics is required to quantitatively reproduce experimental results.

## ■ ASSOCIATED CONTENT

### ■ Supporting Information

The Supporting Information is available free of charge on the ACS Publications website at DOI: 10.1021/acs.jpca.5b07682.

Cartesian coordinates of all the optimized structures (PDF)

## ■ AUTHOR INFORMATION

### Corresponding Author

\*E-mail: morokuma@fukui.kyoto-u.ac.jp. Phone: +81-75-711-7843.

### Notes

The authors declare no competing financial interest.

## ■ ACKNOWLEDGMENTS

The authors are grateful to Dr. Yu Harabuchi for his discussion on the SF-TDDFT method. This work was partly supported by Grants-in-Aid for Scientific Research (A) (No. 24245005 and 15H02158) to K.M. at Kyoto University. The Computer resources at the Academic Center for Computing and Media Studies (ACCMS) at Kyoto University and the Research Center of Computer Science (RCCS) at the Institute for Molecular Science are also acknowledged.

## ■ REFERENCES

- (1) Yuan, C.; Saito, S.; Camacho, C.; Irle, S.; Hisaki, I.; Yamaguchi, S. A  $\pi$ -Conjugated System with Flexibility and Rigidity That Shows Environment-Dependent RGB Luminescence. *J. Am. Chem. Soc.* **2013**, *135*, 8842–8845.
- (2) Yuan, C.; Saito, S.; Camacho, C.; Kowalczyk, T.; Irle, S.; Yamaguchi, S. Hybridization of a Flexible Cyclooctatetraene Core and Rigid Aceneimide Wings for Multiluminescent Flapping  $\pi$  Systems. *Chem.—Eur. J.* **2014**, *20*, 2193–2200.
- (3) Yarkony, D. R. Diabolical Conical Intersections. *Rev. Mod. Phys.* **1996**, *68*, 985.

(4) Yarkony, D. R. Conical Intersections: Diabolical and Often Misunderstood. *Acc. Chem. Res.* **1998**, *31*, 511–518.

(5) Bernardi, F.; Olivucci, M.; Robb, M. A. Potential Energy Surface Crossings in Organic Photochemistry. *Chem. Soc. Rev.* **1996**, *25*, 321–328.

(6) Sobolewski, A. L.; Domcke, W.; Dedonder-Lardeux, C.; Jouvet, C. Excited-state Hydrogen Detachment and Hydrogen Transfer Driven by Repulsive  $1\pi\sigma^*$  States: A New Paradigm for Nonradiative Decay in Aromatic Biomolecules. *Phys. Chem. Chem. Phys.* **2002**, *4*, 1093–1100.

(7) Levine, B. G.; Martínez, T. J. Isomerization Through Conical Intersections. *Annu. Rev. Phys. Chem.* **2007**, *58*, 613–634.

(8) Nanbu, S.; Ishida, T.; Nakamura, H. Future Perspectives of Nonadiabatic Chemical Dynamics. *Chemical Science* **2010**, *1*, 663.

(9) Ohno, K.; Maeda, S. Global Reaction Route Mapping on Potential Energy Surfaces of Formaldehyde, Formic Acid, and Their Metal-Substituted Analogues. *J. Phys. Chem. A* **2006**, *110*, 8933.

(10) Maeda, S.; Morokuma, K. A Systematic Method for Locating Transition Structures of  $A+B\rightarrow X$  Type Reactions. *J. Chem. Phys.* **2010**, *132*, 241102.

(11) Maeda, S.; Ohno, K.; Morokuma, K. Updated Branching Plane for Finding Conical Intersections without Coupling Derivative Vectors. *J. Chem. Theory Comput.* **2010**, *6*, 1538–1545.

(12) Maeda, S.; Ohno, K.; Morokuma, K. Systematic Exploration of the Mechanism of Chemical Reactions: the Global Reaction Route Mapping (GRRM) Strategy Using the ADDF and AFIR Methods. *Phys. Chem. Chem. Phys.* **2013**, *15*, 3683.

(13) Harabuchi, Y.; Maeda, S.; Taketsugu, T.; Minezawa, N.; Morokuma, K. Automated Search for Minimum Energy Conical Intersection Geometries between the Lowest Two Singlet States  $S_0/S_1$ -MECIs by the Spin-Flip TDDFT Method. *J. Chem. Theory Comput.* **2013**, *9*, 4116–4123.

(14) Maeda, S.; Harabuchi, Y.; Taketsugu, T.; Morokuma, K. Systematic Exploration of Minimum Energy Conical Intersection Structures near the Franck–Condon Region. *J. Phys. Chem. A* **2014**, *118*, 12050.

(15) Maeda, S.; Taketsugu, T.; Ohno, K.; Morokuma, K. From Roaming Atoms to Hopping Surfaces: Mapping Out Global Reaction Routes in Photochemistry. *J. Am. Chem. Soc.* **2015**, *137*, 3433.

(16) Andersson, K.; Malmqvist, P.-Å.; Roos, B. O.; Sadlej, A. J.; Wolinski, K. Second-order Perturbation Theory with a CASSCF Reference Function. *J. Phys. Chem.* **1990**, *94* (14), 5483–5488. Finley, J.; Malmqvist, P.-Å.; Roos, B. O.; Serrano-Andrés, L. The Multi-state CASPT2 Method. *Chem. Phys. Lett.* **1998**, *288*, 299–306.

(17) Nakano, H. Quasidegenerate Perturbation Theory with Multiconfigurational Self-consistent-field Reference Functions. *J. Chem. Phys.* **1993**, *99*, 7983.

(18) Shao, Y.; Head-Gordon, M.; Krylov, A. I. The Spin-flip Approach within Time-Dependent Density Functional Theory: Theory and applications to diradicals. *J. Chem. Phys.* **2003**, *118*, 4807.

(19) Minezawa, N.; Gordon, M. S. Optimizing Conical Intersections by Spin-Flip Density Functional Theory: Application to Ethylene. *J. Phys. Chem. A* **2009**, *113*, 12749.

(20) Minezawa, N.; Gordon, M. Photoisomerization of Stilbene: A Spin-Flip Density Functional Theory Approach. *J. Phys. Chem. A* **2011**, *115*, 7901–7911.

(21) Isegawa, M.; Truhlar, D. G. Valence Excitation Energies of Alkenes, Carbonyl Compounds, and Azabenzenes by Time-Dependent Density Functional theory: Linear response of the ground state compared to collinear and noncollinear spin-flip TDDFT with the Tamm-Dancoff approximation. *J. Chem. Phys.* **2013**, *138*, 134111.

(22) (a) Schmidt, M. W.; Baldridge, K. K.; Boatz, J. A.; Elbert, S. T.; Gordon, M. S.; Jensen, J. H.; Koseki, S.; Matsunaga, N.; Nguyen, K. A.; Su, S. J.; Windus, T. L.; Dupuis, M.; Montgomery, J. A. General Atomic and Molecular Electronic Structure System. *J. Comput. Chem.* **1993**, *14*, 1347. (b) Gordon, M. S.; Schmidt, M. W., Advances in electronic structure theory: GAMESS a decade later. In *Theory and Applications of Computational Chemistry: The First Forty Years*; Dykstra,



C. E., Frenking, G., Kim, K. S., Scuseria, G. E., Eds.; Elsevier: Amsterdam, The Netherlands, 2005; p 1167.

(23) Maeda, S.; Osada, Y.; Morokuma, K.; Ohno, K. *GRRM version 1.30, a program for Global Reaction Route Mapping*; 2011.

(24) Tachibana, A.; Fukui, K. Differential Geometry of Chemically Reacting Systems. *Theoretica chimica acta* **1978**, *49*, 321.

(25) Garavelli, M.; Bernardi, F.; Cembran, A.; Castaño, O.; Frutos, L. M.; Merchán, M.; Olivucci, M. Cyclooctatetraene Computational Photo- and Thermal Chemistry: A Reactivity Model for Conjugated Hydrocarbons. *J. Am. Chem. Soc.* **2002**, *124*, 13770–13789.

(26) Bearpark, M. J.; Bernardi, F.; Clifford, S.; Olivucci, M.; Robb, M. A.; Vreven, T. Cooperating Rings in *cis*-Stilbene Lead to an  $S_0/S_1$  Conical Intersection. *J. Phys. Chem. A* **1997**, *101*, 3841–3847.

(27) Jacquemin, D.; Wathelet, V.; Perpète, E. A.; Adamo, C. Extensive TD-DFT Benchmark: Singlet-Excited States of Organic Molecules. *J. Chem. Theory Comput.* **2009**, *5*, 2420–2435.